Romanian Reports in Physics **72**, 415 (2020)

ANTIREFLECTION COATINGS COMPRISED OF METAL NANOPARTICLES AND SILICON NITRIDE

MUIN F. UBEID[1,*], MOHAMMED M. SHABAT[1], JOEL CHARRIER[2]

[1] Islamic University of Gaza, Faculty of Science, Department of Physics, P.O. 108, Gaza, Gaza Strip, Palestinian Authority
[*]Email: *mubeid@mail.iugaza.edu*
[2] Université de Rennes 1, Laboratoire FOTON, UMR-CNRS 6082, CCLO, ENSSAT BP80518, F-22305 Lannion Cedex, France

Received July 27, 2020

Abstract. An antireflection coating structure comprised of metal (copper) nanoparticles over silicon nitride has been numerically investigated. The structure is embedded between semi-infinite vacuum and silicon substrate and a TE plane polarized wave is incident on the proposed structure. The permittivity of all the involved materials in the proposed structure is wavelength dependent. Numerical results are presented to show the effects of the incidence angle, the wavelength, and the structure parameters on the reflection coefficient. The antireflection coating structure and the obtained results could be useful for design of future solar cells and optical sensors.

Key words: metal nanoparticles, antireflection coatings, silicon nitride, solar cells, optical sensors.

1. INTRODUCTION

Nanoparticles are particles between 1 and 100 nanometers (nm) in size with a surrounding interfacial layer. The interfacial layer typically consists of ions, inorganic, and organic molecules [1, 2]. Nanoparticles exist in the natural world and are also created as a result of human activity [3]. They can be classified into any of various types, according to their size, shape, and material properties. Some classifications distinguish between organic and inorganic nanoparticles [4]. Other classifications divide nanoparticles according to whether they are carbon-based, ceramic, semiconductors, or polymeric [5]. In addition, nanoparticles can be classified as hard (*e.g.* titania, silica particles, and fullerenes) or as soft (*e.g.* liposomes, vesicles, and nanodroplets) [6]. The specifications of nanoparticles typically depend on their applications, such as in diagnosis or thereby *versus* basic research, or may be related to the way in which they were produced. Nanoparticles have gained a high reputation in recent decades due to their diverse applications. They can also contribute to stronger, lighter, cleaner, and "smarter" surfaces and systems. Nanoparticles are already being used in the manufacture of scratch proof eyeglasses, crack-resistant

paints, anti-graffiti coatings for walls, transparent sunscreens, and ceramic coatings for solar cells [7, 8]. Nanomaterials are also used in biology and medicine in a wide variety of ways. Examples include products of drug delivery and gene therapy, tissue engineering, DNA probes, and nanoscale biochips [9, 10].

Antireflection coating (ARC) is a type of optical coating applied to the surface of lenses and other devices elements to reduce reflection [11, 12]. Light that is reflected at the coating-substrate interface will be half wavelength out of phase from the incident light that is reflected from the coating-air interface, resulting in destructive interference and reduce reflectance [13]. A special application of an antireflection coating is on solar cells to reduce the reflection losses that reduce efficiency [14]. Reflected light reduces the number of photons that can be used to form the electron-hole pairs that drive the current in solar cells [15]. Various structure models based on conventional nanoparticles [16–22] and more recently on conductive nanoparticles [23–24] have been utilized to enhance the solar cells efficiency.

Shabat and Ubeid [25] have theoretically investigated the optical reflection properties of a periodic metamaterial-dielectric multilayered structure. They reported that the structure is an antireflection coating if it is placed between two semi-infinite media of the same kind and the two slabs that constitute each period have the same width and opposite refractive indices. Khan *et al.* [26] have reviewed antireflection coatings. They have analyzed and evaluated critically the progress and recent development in the fabrication of ARC thin films comprising organic coatings, inorganic coatings, polymer ARC, and bionic ARC. Han *et al*. [27] have fabricated by layer-by-layer assembly of layered double hydroxide nanoparticles and poly (sodium-sulfonate) followed by calcinations, which exhibited properties of both antireflection and antifogging. Garshin and Aiko-Shvaikovski [28] have studied theoretically the defect formation process in silicon nitride and Groep *et al*. [29] have demonstrated effective nanopatterned antireflection coating on glass that is based on sol-gel and large-area substrate-conformal soft-imprent technology. Zhang *et al.* [30] have reported a self-cleaning particle coating with antireflection properties. The coating was prepared by depositing SiO_2 single-layered particle coatings on polyelectrolyte-modified glass substrates through electrostatic attraction, then depositing another layer of TiO_2. Xu *et al*. [31] have developed a facile dip-coating to fabricate visible/near-IR antireflective and superhydrophobic coatings from hydrophobically modified hollow silica nanoparticles and pol (methyl methacrylate). Bouhafs *et al*. [32] have presented reflectance calculation for various single, double, and triple-layer antireflection coatings to determine the optimum thickness and the refractive index of each layer at a single wavelength for optoelectronic applications and through the visible spectrum for photovoltaic applications.

In this study, it is intended to create an antireflection coating comprised of metal (copper) nanoparticles and silicon nitride. The structure that is placed between semi-infinite vacuum and silicon substrate is designed for solar energy

applications. We consider that a TE-polarized plane wave is incident through vacuum on the structure. The electric and magnetic fields are determined in each region using Maxwell's equations. Then, the boundary conditions are imposed at each interface and Snell's law is used to obtain the reflection coefficients in terms of Fresnel amplitudes. The overall reflectance of the structure is formulated in terms of these amplitudes. Finally, the numerical results show the effect of the structure parameters, the layer thickness, the incidence angle, and the wavelength on the reflected power of the structure.

The paper is structured as follows. In Section 2 we briefly present the antireflection coating structure and the theoretical method used to calculate its reflected power (reflectance). We discuss in Section 3 the results of numerical calculations for the reflectance and its dependence of the incident radiation wavelength and the parameters describing the antireflection coating structure. The summary and a brief discussion of the obtained results are given in Section 4.

2. ANTIREFLECTION COATING STRUCTURE AND ITS REFLECTANCE

Figure 1 shows a single layer of spherical metal nanoparticles embedded in air. The letters r, P, d, L_1, and L_2 stand for the radius of the particles, the period of the arrays, the thickness of the layer (equals the particle diameter), the width of the layer, and the length of the layer, respectively.

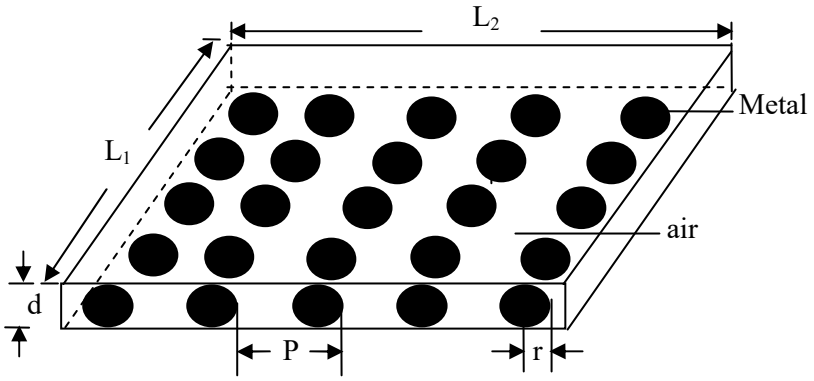

Fig. 1 – Schematic representation of a single layer of spherical metal nanoparticles embedded in air.

Figure 2 shows four regions, each with permittivity ε_ℓ and permeability μ_ℓ, where ℓ represents the region order. Region 1 is a vacuum ($\varepsilon_1 = \varepsilon_o$, $\mu_1 = \mu_o$) filling the region $z < 0$, Region 2 is metal nanoparticles (ε_2 , μ_2) restricted to the limits $z = 0$ to $z = d_2$, Region 3 is silicon nitride (ε_3, μ_3) extended from $z = d_2$ to $z = d_2 + d_3$,

Region 4 is silicon (ε_4, μ_4) filling the region $z > d_2 + d_3$. A transverse-electric polarized plane wave (TE wave) in Region 1 is incident on the plane $z = 0$ at some angle θ relative to the normal to the boundary (see Fig. 2).

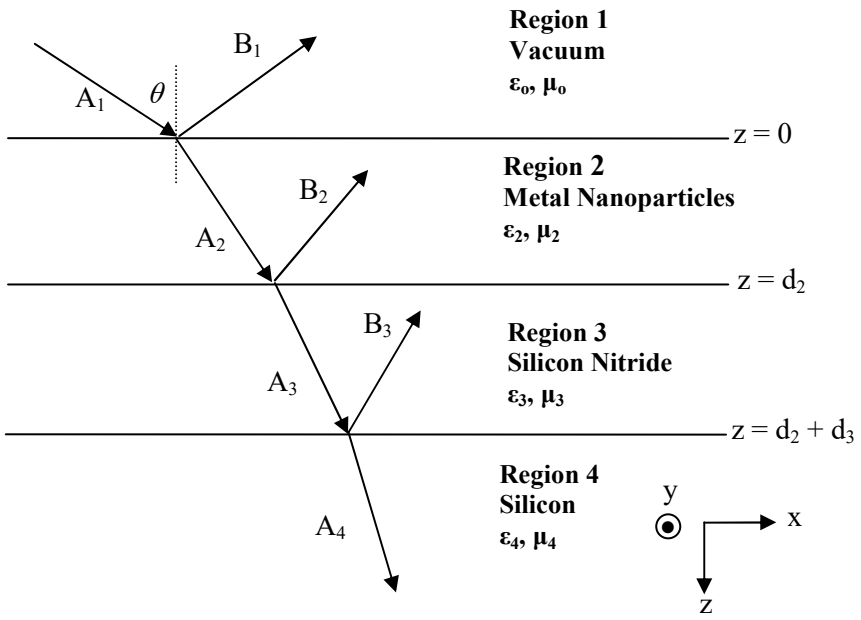

Fig. 2 – Antireflection coating structure comprised of metal nanoparticles and silicon nitride embedded between semi-infinite vacuum and silicon substrate.

The electric field in each region is:

$$\vec{E}_\ell = \left(A_\ell e^{ik_{\ell z}z} + B_\ell e^{-ik_{\ell z}z} \right) \; e^{i(k_{\ell x}x - \omega t)} \quad \hat{y}. \tag{1}$$

To find the corresponding magnetic field $\vec{H}_\ell$, we start with Maxwell's equation $\vec{\nabla} \times \vec{E}_\ell = -\partial \vec{B} / \partial t$. Substituting $\vec{B} = \mu_\ell \vec{H}_\ell$ and solving for $\vec{H}_\ell$ yield:

$$\vec{H}_\ell = \frac{1}{\mu_\ell \omega} \left[(A_\ell k_{\ell x} e^{ik_{\ell z}z} + B_\ell k_{\ell x} e^{-ik_{\ell z}z})\hat{z} + (-A_\ell k_{\ell z} e^{ik_{\ell z}z} + B_\ell k_{\ell z} e^{-ik_{\ell z}z})\hat{x} \right] \; e^{i(k_{\ell x}x - \omega t)}, \tag{2}$$

where A_ℓ and B_ℓ are the amplitude of forward and backward traveling waves (ℓ = 1, 2, 3, 4) , $k_\ell = n_\ell \omega / c$ is the wave vector inside the material, and n_ℓ is the refractive index of it. Also, the subscripts x and z represent the x- and z-components of the corresponding wave numbers, respectively.

Then we apply the boundary conditions for $\vec{E}$ and $\vec{H}$ fields at each layer interface, that is, at $z = 0$, $E_{1y} = E_{2y}$ and $H_{1x} = H_{2x}$ and so on. This yields six equations with six unknown parameters as [33]:

$$A_1 + B_1 = A_2 + B_2 \tag{3}$$

$$\frac{k_{1z}}{\mu_1}\left(A_1 - B_1\right) = \frac{k_{2z}}{\mu_2}\left(A_2 - B_2\right) \tag{4}$$

$$A_2 e^{ik_{2z}d_2} + B_2 e^{-ik_{2z}d_2} = A_3 e^{ik_{3z}d_2} + B_3 e^{-ik_{3z}d_2} \tag{5}$$

$$\frac{k_{2z}}{\mu_2}\left(A_2 e^{ik_{2z}d_2} - B_2 e^{-ik_{2z}d_2}\right) = \frac{k_{3z}}{\mu_3}\left(A_3 e^{ik_{3z}d_2} - B_3 e^{-ik_{3z}d_2}\right) \tag{6}$$

$$A_3 e^{ik_{3z}(d_2+d_3)} + B_3 e^{-ik_{3z}(d_2+d_3)} = A_4 e^{ik_{4z}(d_2+d_3)} \tag{7}$$

$$\frac{k_{3z}}{\mu_3}\left(A_3 e^{ik_{3z}(d_2+d_3)} - B_3 e^{-ik_{3z}(d_2+d_3)}\right) = \frac{k_{4z}}{\mu_4} A_4 e^{ik_{4z}(d_2+d_3)}. \tag{8}$$

Here $k_{1x} = k_{2x} = k_{3x} = k_{4x} \equiv$ Snell's law and:

$$k_{\ell z} = \frac{\omega}{c}\sqrt{n_\ell^{\,2} - n_1^{\,2}\sin^2\theta}. \tag{9}$$

The Fresnel coefficients (interface reflection and transmission coefficients r, t, respectively) for TE-polarized light are calculated as [34, 35]:

$$r_{ij} = \frac{\mu_j k_{iz} - \mu_i k_{jz}}{\mu_j k_{iz} + \mu_i k_{jz}}, \tag{10}$$

$$t_{ij} = \frac{2\mu_j k_{iz}}{\mu_j k_{iz} + \mu_i k_{jz}}, \tag{11}$$

where i, j corresponds to any of two adjacent media.

The reflection coefficient r of the structure is given by [36, 37]:

$$r = \frac{B_1}{A_1} = \frac{r_{12} + r_{12}r_{23}r_{34}e^{i2k_{3z}d_3} + r_{23}e^{i2k_{2z}d_2} + r_{34}e^{i2(k_{2z}d_2 + k_{3z}d_3)}}{1 + r_{23}r_{34}e^{i2k_{3z}d_3} + r_{12}r_{23}e^{i2k_{2z}d_2} + r_{12}r_{34}e^{i2(k_{2z}d_2 + k_{3z}d_3)}} \tag{12}$$

The reflected power R (reflectance) of the structure is related to the reflection coefficient r as:

$$R = |r|^2. \tag{13}$$

3. NUMERICAL RESULTS

In this Section we calculate the reflectance of the structure shown in Fig. 2 *versus* the light wavelength, the angle of incidence, the period thickness, and silicon nitride thickness when the nanoparticle radius changes. In order to verify the numerical calculations, we have compared our results with those reported in Ref. [38], where silicon nanoparticles have been used in region 2. Therefore, it can be said that the results achieved in this study are in a good agreement and are compatible with the results obtained in Ref. [38].

In the calculations, the metal type of the nanoparticles in region 2 is selected to be copper (Cu). The permittivity and refractive index of the copper can be calculated from the Drude model as [39]:

$$\varepsilon_i(\lambda) = 1 - \frac{\lambda^2 \lambda_c^{\,2}}{\lambda_p^{\,2}(\lambda_c + i\lambda)}, \tag{14}$$

$$n_i(\lambda) = \sqrt{\varepsilon_i(\lambda)}, \tag{15}$$

where λ is the wavelength of the incident radiations, and λ_p and λ_c are the plasma wavelength and the collision wavelength of the metal, respectively. The following parameters appearing in [36] are used, for Cu:

$$\lambda_p = 1.3617 \times 10^{-7} \text{ m}, \lambda_c = 4.0852 \times 10^{-5} \text{ m}.$$

The Maxwell-Garentt effective medium approximation is used to calculate the effective permittivity of the composite materials in region 2 formed by metal (copper) nanoparticles in air, this effective permittivity ε_2 is given by [16, 38]:

$$\varepsilon_2 = \varepsilon_b \frac{\varepsilon_i(1+2f) + 2\varepsilon_b(1-f)}{\varepsilon_i(1-f) + \varepsilon_b(2+f)}, \tag{16}$$

where ε_b is the permittivity of the base material (air), ε_i is the permittivity of the particle's materials (copper) and f is the volume fraction of the particles in the base medium. For a layer of thickness d_2, its volume can be expressed as $V_{\text{layer}} = L_1 \times L_2 \times d_2$. For simplicity, we take $L_1 = L_2 = 1$ cm. The volume of a spherical particle of radius r is

$V_p = 4\pi r^3/3$. The number of particles on the surface can be expressed as $N_p = (L_1/P) \times (L_2/P)$. Thus, the volume fraction of the particles in the corresponding layer is $f = (N_p \times V_p)/V_{layer}$.

The optical data for silicon are taken from [40]. For silicon nitride (Si_3N_4) in region 3, its permittivity is a function of wavelength λ described by the equation [38]:

$$\varepsilon_3 = 11.67316 + \frac{1}{\lambda^2} + \frac{.004482633}{\lambda^2 - 1.108205^2}. \tag{17}$$

In the computation, the operating wavelength is chosen to be 500 nm. The operating wavelength is chosen by arbitrary decision to be near the center of the visible spectrum. The thickness of copper nanoparticles (Cu-NPs) layer in region 2 is assumed to be equal to the particle diameter, $d_2 = 2r$ [38]. The permeability of any region given in Fig. 2 is assumed to be equal to the permeability of free space, $\mu_\ell = \mu_\infty$.

To check the effect of the Cu-NPs layer on the reflection properties of the structure, Fig. 3 shows the reflectance as a function of the wavelength of the incident radiation for normal incidence. The calculations are performed for bare surface, Si_3N_4 with thickness 60 nm on silicon surface, and Cu-NPs with period 450 nm and diameter 125 nm over Si_3N_4 layer and Si surface. The wavelength of the incident radiations is changed between 300 nm and 1100 nm, that is in visible and near-infrared ranges. It can be seen that strong reduction of the reflection is observed by inducing the Cu-NPs layer with the combination of Si_3N_4 and Si surface. The effect of the Cu-NPs is observed for wavelengths greater than 500 nm.

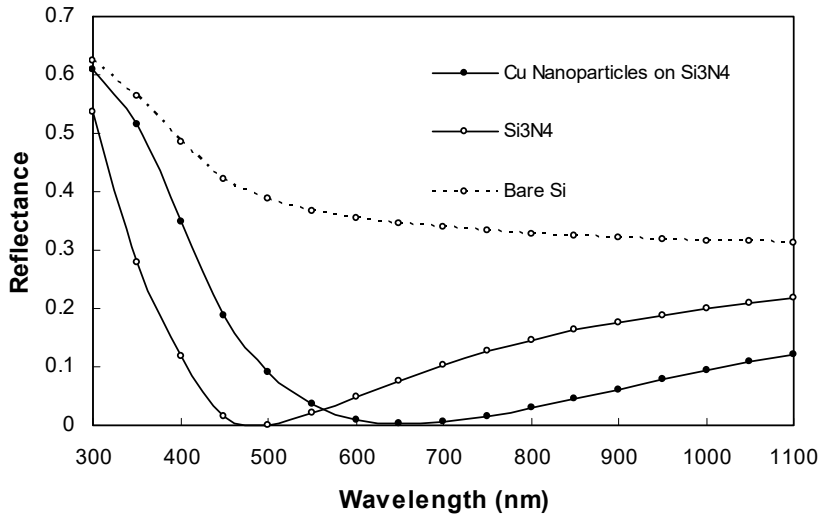

Fig. 3 – Reflectance as a function of the wavelength of the incident radiation for bare Si surface, Si_3N_4 layer combined with Si surface, and Cu-NPs layer with the combination of Si_3N_4 and Si surface.

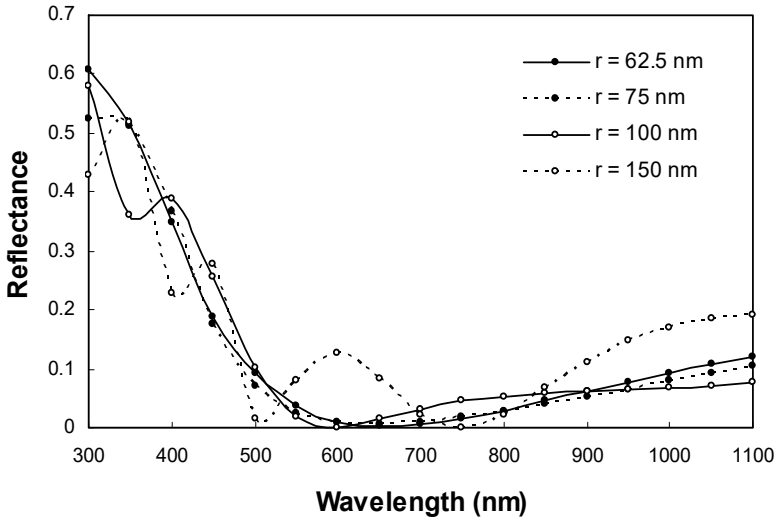

Fig. 4 – The reflectance as a function of wavelength of the incident radiation when the nanoparticle radius changes, r = 62.5 nm, 75 nm, 100 nm, and 150 nm.

Figure 4 shows the reflectance *versus* the operating light wavelength at normal light incidence when the nanoparticle radius changes, r = 62.5 nm, 75 nm, 100 nm, and 150 nm. The thickness of the silicon nitride in region 3 is equal to 60 nm and the period size in region 2 is equal to 450 nm. We see that the reflectance has a smooth behavior for radii 62.5 nm and 70 nm. It shows a nonlinear characteristic and variable properties when the nanoparticle radius increases.

Figure 5 presents the reflectance *versus* the period for 500 nm wavelength and for four values of the radius of the nanoparticle, r = 62.5 nm, 75 nm, 100 nm, and 150 nm. The period size is changed from 0 nm to 1000 nm. The angle of incidence and the thickness of the silicon nitride are kept the same as in Fig 4. As it seen from the figure, the reduced reflectance region is wider for small radii. There are more ripples in the period behavior of the reflectance when the radius increases. In addition, the symmetry shifts in period to the right when the radius has increased.

Figure 6 illustrates the variation of reflectance with the angle of incidence for 500 nm wavelength when the radius of the nanoparticle's changes. The angle of incidence is changed between 0° and 90° to realize all possible angles of incidence. The thickness of the silicon nitride and the size of the period are kept the same as in Fig. 4. It is found that the incidence angle band is wider for reduced reflectance for r = 62.5 nm, 75 nm, and 100 nm and is narrower for r = 150 nm.

Figure 7 presents the reflectance *versus* the thickness of the silicon nitride for 500 nm wavelength and for different values of the radius of the nanoparticles, r = 62.5 nm, 75 nm, 100 nm, 150 nm. The thickness of the silicon nitride is adjusted and tuned to be between 0 nm to 120 nm. The angle of incidence and the

period are similarly kept as in Fig. 4. It is observed that a nearly zero reflectance is achieved at 60 nm silicon nitride thickness for r = 62.5 nm, 75 nm, and 100 nm and at 75 nm silicon nitride thickness for r = 150 nm.

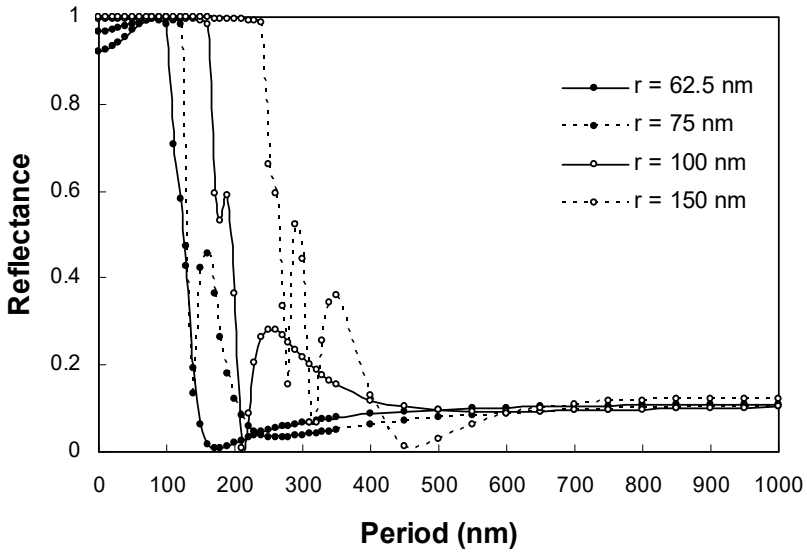

Fig. 5 – The reflectance at 500 nm wavelength *versus* the period for different values of the radius of the nanoparticle, r = 62.5 nm, 75 nm, 100 nm, and 150 nm.

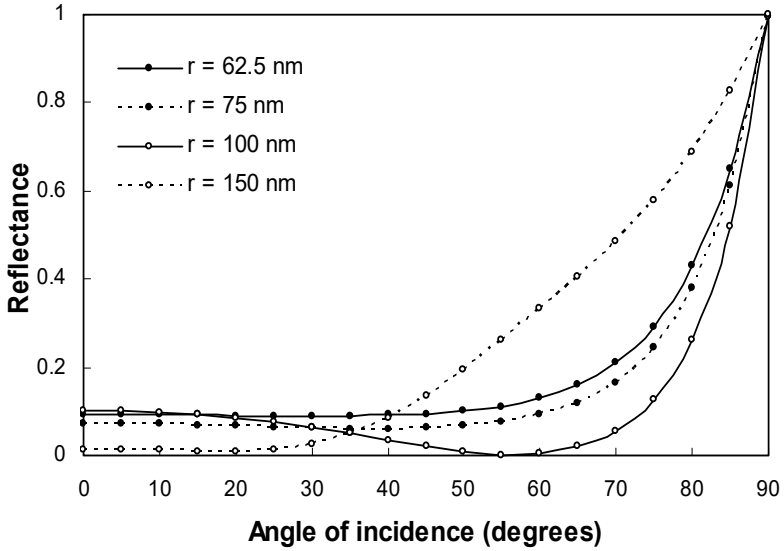

Fig. 6 – The variation of reflectance at 500 nm wavelength with the angle of incidence for different values of the nanoparticle radius, r = 62.5 nm, 75 nm, 100 nm, and 150 nm.

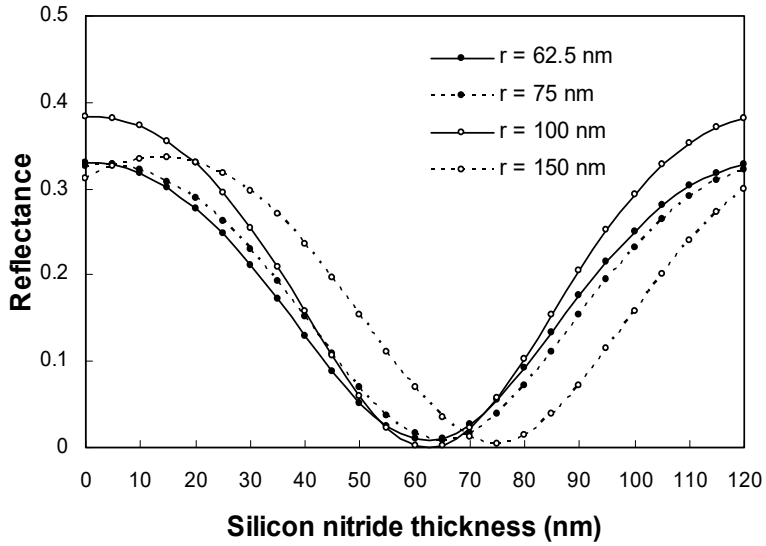

Fig. 7 – The reflectance at 500 nm wavelength versus the thickness of the silicon nitride for different values of the nanoparticle radius, r = 62.5 nm, 75 nm, 100 nm, and 150 nm.

4. CONCLUSIONS

We have numerically studied an antireflection coating structure containing metal nanoparticles over silicon nitride. The reflectance *versus* the wavelength, the angle of incidence, the period size, and the thickness of the silicon nitride have been investigated and studied numerically to observe the effects of the nanoparticle radius on them. As it can be seen from the theoretical and the numerical results, if the nanoparticle radius changes, the characteristic of the reflection will be affected by this change. A very low reflection in the mentioned wavelength ranges is observed for Cu-NPs optimal parameters (radii 62.5 and 75 nm, period 450 nm) with 60 nm thickness of the silicon nitride. Moreover, the stability of the reflection for oblique incidence is observed for angles lower than 60°. The obtained results could be helpful to the researchers and designers working in the area of solar energy applications.

Acknowledgements. The author (MMSh) acknowledges financial support from Alquds Academy for Scientific Research, Palestine. The author (JC) and (MMSH) acknowledge financial support from PHC AL MAQDISI 2019.

REFERENCES

1. C. A. Batista, R. A. Larson, and N. A. Kotov, *Nanoditivity of nanoparticles interactions*, Science **350** (6257), 1242477 (2015).
2. M. Vert, Y. Doi, K. H. Hellwich, M. Hess, P. Hodge, P. Kubisa, M. Rinaudo, and F. Schue, *Technology for biorelated polymers and applications*, Pure and Applied Chemistry **84** (2), 377–410 (2012).

3. A. D. MacNaught, A. Wilkinson, *Compendium of chemical Terminology*, 2nd Edition, Blackwell Science Publications, Oxford, 1997.
4. J. Aleman, A. V. Chadwick, J. He, M. Hess, K. Horie, R. C. Jones, P. Kratochvil, I .Meisel, I. Mita, G. Moad, S. Penczek, and R. F. T. Stepto, *Definitions of terms relating to the structure and processing of sols, gels networks, and inorganic-organic hybrid materials*, Pure and Applied Chemistry **79** (10), 1801–1829 (2007).
5. C. Buzea, I. I. Pacheco, and K. Robbie, *Nanomaterials and nanoparticles: sources and toxicity*, Biointerphases **2** (4), MR17–MR71 (2007).
6. C. G. Granqvist, R. A. Buchrman, J. Wyns, and A. J. Sievers, *Far-infrared absorption in Ultrafine Al Particles,* Phys. Rev. Lett. **37** (10), 625–629 (1976).
7. Y. L. Hewakuruppu, L. A. Dombrovsky, C. Chuyang, V. Timchencho, X. Jiang, S. Baek, and R. A. Taylor, *Plasmonic pump-probe method to study semi-transparent nanofluids*, Appl. Opt. **52** (24), 6041–6050 (2013).
8. S. I. Thakore, P. S. Nagarj, R. N. Jadeja, M. Thounaojam, R. V. Devkar, and P. S. Rathore, *Sapota fruit latex mediated synthesis of Ag, Cu mono and bimetallic nanoparticles and their in vitro toxicity studies*, Arabian Journal of Chemistry **15** (5) , 694–700 (2019).
9. A. P. Nikalje, *Nanotechnology and its applications in medicine*, Medicinal Chemistry **5**, 81–89 (2015).
10. M. Kot, L. Major, J. M. Lackner, K. C. Przywara, M. Janusz, and W. Rakowski, *Mechanical and tribological properties of carbon-based graded coatings*, J. Nanomaterials **2016**, 8306345 (2016).
11. M. F. Ubeid, M. M. Shabat, and D. M. Schaadt, *Wide-angle and wavelength-independent perfect absorption at metamaterial surfaces*, Rom. Rep. Phys. **68** (2), 725–735 (2016).
12. A. Deinega, I. Valuev, B. Potapkin, and Y. Lozovik, *Minimizing of light reflection from dielectric textured surface*, J. Opt. Soc. Am. A **28**, 770–777 (2011).
13. R. A. Serway and J. W. Jewett, *Physics for Scientists and Engineers*, Books/Cole Publishing Co. USA ch. 36, p. 1189. 2003.
14. M. F. Ubeid, and M. M. Shabat, *High efficiency solar cells of multilayered organic structures*, Journal of Nanoelectronics and Optoelectronics **13** (8), 1175–1180 (2018).
15. M. F. Ubeid, and M. M. Shabat, *High efficiency solar cells with multilayered structures containing graphene*, Chinese J. Phys. **56** (5), 2589–2596 (2018).
16. M. M. Shabat, D. M. El-Amassi, and D. M. Schaadt, *Design and analysis of multilayer waveguides with different substrate media and nanoparticles for solar cells*, Solar Energy Journal **137**, 409–412 (2016).
17. Hala El-Khozendar, Rifa J. El-Khozondar, M. M. Shabat, D. M. Schaadt, *Solar cell with multilayer structure based on nanoparticles composite*, Optik **166**, 127–132 (2018).
18. Kh. Kh. AbuShaar, M. M. Shabat, D. M. El-Amassi, and D. M. Schaadt, *Optimization Design of Solar Cell Based on Silver Nanoparticles*, Journal of Nanoelectronics and Optoelectronics, **14** (9), 1237–1241 (2019).
19. Kh. Kh. AbuShaar, M. M. Shabat, Dena M. El-Amassi, and D. M. Schaadt, *Enhancement of Solar Cell Using Two-Nanoparticles (Ag-Au)*, Modern Phys. Lett. **33** (24), 1950289 (2019).
20. S. A. Nassar, M. M. Shabat, D. M. Schaadt, *Simulation of three types of Nanoparticles on solar cell structure model*, International J. Modern Physics **34** (7), 2050054 (2020).
21. B. Singh, M. M. Shabat, and D. M. Schaadt, *Analytical modelling of power transfer via metallic nanoparticles in a solar cell absorber*, Journal of Quantitative Spectroscopy and Radiative Transfer **243**, 106807 (2020).
22. B. Singh, M. M. Shabat, D. M. Schaadt, *Wide angle antireflection in metal nanoparticles embedded in a dielectric matrix for plasmonic solar cells*, Progress in Photovoltaics: Research and Applications **28** (7), 682– 690 (2020).
23. H. M. Mousa, M. M. Shabat, A. K. Ouda, and D. M. Schaadt, *Enhanced absorption of TM waves in Conductive nanoparticles structure*, Modern Phys. Lett. B **32** (15), 1850163 (2018).
24. H. M. Mousa, M. M. Shabat and A. K. Ouda, *Anti-reflection coating solar cell structure based on conductive nanoparticles*, J. Science and Engineering B **7** (9–10), 229–236 (2017).

25. M. M. Shabat and M. F. Ubeid, *Antireflection coating at metamaterial waveguide structure for solar energy applications*, Energy Procedia **50**, 314–321 (2014).
26. S. B. Khan, H. Wu, C. Pan, and Z. Zhang, *A mini review: Antireflection coatings processing technique, applications and future perspective*, Research and Review: J. of Material Science **5** (4), 36–54 (2017).
27. J. Han, Y. Dou, M. Wei, D. G. Evans, and X. Duan, *Antireflection/antifogging coatings based on nanoporous films derived from layered double hydroxide*, Chemical and Engineering J. **169**, 371–378 (2011).
28. A. P. Garshin and V. E. Aiko-Shvaikovski, *Theoretical analysis of defect formation process in silicon nitride*, Refractive and Industrial Ceramics **39**, 169–176 (1998).
29. J. de Groep, P. Spinelli, and A Polman, *Single-step soft-imprinted large-area nanopatterned antireflection coatings*, Nano Lett. **15** (6), 4223–4228 (2015).
30. X. T. Zhang, O. Sato, M. Taguchi, Y. Einaga, T. Murakami, and A. Fujishima, *Self-cleaning particle coating with antireflection properties*, Chemistry and Materials **17**, 696–700 (2003).
31. L. Xu, L. Gao, and J. He, *Fabrication of visible/near-IR antireflective and superhydrophobic coatings from hydrophobically modified hollow silica nanoparticles and pol (methyl methacrylate)*, RSC Adv. **2**, 12764–12769 (2012).
32. D. Bouhafs, A. Moussi, A. Chikouche, and M. Ruiz, *Design and simulation of antireflection coating systems for optoelectronic devices: application to silicon solar cells*, Solar Energy Materials and Solar Cells **52**, 77–93 (1998).
33. M. F. Ubeid, *Reflection and transmission of electromagnetic waves by a layered structure containing left-handed material*, Thesis (PhD), Sudan University for Science and Technology, 2013.
34. M. F. Ubeid and M. M. Shabat, *Numerical study of antireflection coatings in waveguide structures with silicon nanoparticles interlayer*, J. Mod. Opt. **64** (4), 374–378 (2017).
35. M. F. Ubeid and M. M. Shabat, *Analytical sensitivity and reflected power through a D-shape optical fiber sensor*, Optoelectronics Rev. **22** (3), 191–195 (2014).
36. M. F. Ubeid and M. M. Shabat, *Numerical investigation of a D-shape optical fiber sensor containing graphene*, Appl. Phys. A **118** (3), 1113–1118 (2015).
37. M. F. Ubeid and M. M. Shabat, *Reflection and transmission of electromagnetic waves by a multilayered solar cell containing organic materials*, Optical and Quantum Electron. **51** (6), 197 (2019).
38. M. F. Ubeid and M. M. Shabat, *Numerical study of antireflection coatings in waveguide structures with silicon nanoparticles interlayer*, J. Mod. Opt. **64** (4), 374–378 (2017).
39. M. F. Ubeid and M. M. Shabat, *Analytical sensitivity and reflected power through a D-shape optical fiber sensor*, Optoelectronics Rev. **22** (3), 191–195 (2014).
40. M. A. Green and M. Keevers, *Optical properties of intrinsic silicon at 300 K*, Progress in Photovoltaics: Research and Applications **3** (3), 189–192 (1995).